Available online at www.sciencedirect.com
ScienceDirect
International Journal of Multiphase Flow 33 (2007) 394–410
International Journal of Multiphase Flow
www.elsevier.com/locate/ijmulflow

# Consistency issues of Lagrangian particle tracking applied to a spray jet in crossflow

Mirko Salewski *, Laszlo Fuchs

*Lund Institute of Technology, Division of Fluid Mechanics, Lund University, 22100 Lund, Sweden*

Received 8 November 2005; received in revised form 27 September 2006

**Abstract**

Numerical simulations are performed for multiphase jets in crossflow. The flow solver uses an Eulerian/Lagrangian approach. Turbulence in the gas phase is modeled in the framework of large eddy simulation. The dispersed phase is handled using Lagrangian particle tracking. The model assumptions of solvers for Lagrangian particle tracking are critically assessed for typical flow conditions of spray jets in crossflow. The droplets are assumed to be spherical and isolated. It is shown that several model assumptions are apparently inconsistent in larger portions of the flow field. Firstly, average Weber numbers can be so large that the model assumption to regard droplets as spherical is questionable, not only near the nozzle, but also in the far-field. Secondly, the average droplet spacing can be so low that droplets directly interact with each other, again also in the far-field. Thirdly, the average Stokes numbers in the jet region can be so large that the phase coupling between the dispersed and continuous phase is weak. Some remedies to these deficiencies are proposed.


*Keywords:* Lagrangian particle tracking; Euler/Lagrange; Spray; Particle interaction; Droplet deformation; Phase coupling

## 1. Introduction

Spray jets in crossflow (JICF) are of interest for application as fuel injection systems in low $NO_x$ burners operating in the lean premixed prevaporized (LPP) combustion mode. A liquid fuel jet is injected into a crossflow of preheated air flow. The liquid jet atomizes to fine droplets which disperse and evaporate quickly. The evaporated fuel mixes with air ideally prior to combustion. Premixed flames are preferable to diffusion flames as they offer the opportunity to chose the equivalence ratio well below or above stoichiometric conditions and thereby reduce local temperatures and $NO_x$ formation rates. While $NO_x$ emissions for gas turbines operating with gaseous fuel are down to single-digit ppm levels (Caraeni et al., 2000), the emissions are significantly higher if liquid fuels are used. This is due to local intermittent non-mixedness which leads to hot spots with

* Corresponding author. Tel.: +46 462221407; fax: +46 462224717.
*E-mail address:* mirko.salewski@vok.lth.se (M. Salewski).
*URL:* www.fm.vok.lth.se (M. Salewski).

0301-9322/$ - see front matter © 2006 Elsevier Ltd. All rights reserved.
doi:10.1016/j.ijmultiphaseflow.2006.09.007

excessive production of thermal $NO_x$. Fuel injection systems for LPP gas turbine combustors are therefore required to steadily provide a homogeneous mixture of fuel and air with an adjusted equivalence ratio profile. A spray JICF is advantageous as fuel injection system since atomization offers the opportunity to disintegrate the liquid fuel jet to fine droplets, which evaporate fast, while the momentum ratio, the injection angle, or swirl can be used to tailor various equivalence ratio profiles.

The Lagrange/Euler description is often applied for simulation of droplet- or particle-laden gas flows. The Eulerian description of the continuous phase handles the turbulence by large eddy simulation (LES). With respect to Lagrangian particle tracking (LPT) this has the distinct advantage that the large scale motions, on which dispersion of the droplets mainly depends (Yeh and Lei, 1981), are simulated while only the small scales are modeled. Turbulence models based on Reynolds-averaged Navier–Stokes (RANS) equations, on the other hand, require also modeling of the large scales. Consequently, the leading effects on droplets dispersion also have to be modeled with RANS-based turbulence models. LPT implies among other things that one assumes that the droplets are spherical, the drag-coefficient is known, and that no inter-particle interaction takes place. The accuracy of these assumptions can be assessed *a posteriori* by examining characteristic parameters of two-phase droplet flows, i.e. the average Weber- and the Stokes numbers as well as the average inter-particle spacing.

The local average inter-particle spacing may vary largely, by more than an order of magnitude. In very dilute flow one-way coupling is enough, in less dilute flow two-way coupling is required. Even smaller inter-particle distances imply that so-called four-way interaction is important (Elghobashi, 1994). Four-way interaction can be divided into direct (collision) and indirect (aerodynamic) interaction. For in-line droplets the aerodynamic inter-droplet coupling has noticeable impacts up to many droplet diameters in the wake of a preceding droplet (Holländer and Zaripov, 2005). The drag coefficient of the second of two in-line particles decreases by 30% for an inter-particle spacing $L/D_p \sim 6$ (Prahl et al., 2006). $L$ is the distance between two particles and $D_p$ the particle diameter. While direct interaction is routinely treated through collision models, aerodynamic interaction in fully coupled multiphase flow computation of turbulent flow is always neglected to present date. Isolated droplets are further assumed in current models for evaporation (Torres et al., 2003) and droplet breakup (Reitz and Diwakar, 1987). Secondly, large Weber numbers imply that the droplets do deform which may mean that modifications in the lift and the drag coefficients are required (Helenbrook and Edwards, 2002; Prahl et al., 2006). This droplet deformation is usually neglected in computations, e.g. in Khosla and Crocker (2004), Becker and Hassa (2002), or Ghosh and Hunt (1998). In recent years some attempts are being made to incorporate the effect of droplet deformation, e.g. Madabhushi (2003). Additionally, the assumption of a spherical droplet is not only used in the computation of the trajectory, but also in recently improved submodels for collision (Schmidt and Rutland, 2000), evaporation (Torres et al., 2003), and breakup (Reitz and Diwakar, 1987). Lastly, large Stokes numbers suggest that the droplets do not follow the continuous phase and the mutual interaction between continuous and dispersed phases is weak.

To give *a posteriori* estimates of these frequently used model assumptions, average Weber numbers, average Stokes numbers, and the average droplet spacing are plotted in this work. The sensitivity to the injection droplet radius, momentum flux ratio, collision, evaporation, and breakup models is assessed. Regions are identified in which the model premises are inconsistent with the results, suggesting that no consistent solution can be obtained. Model inconsistency may therefore be regarded as as strong a driver towards development of new models as dissonance between measurement and computation. In addition to the flow-dependent inconsistencies, there is an inherent inconsistency in the Eulerian/Lagrangian description of any problem. In single-phase flow, it is argued that the algebraic equations approach the partial differential equations in the limit of zero cell size (so-called consistency in Lax' equivalence theorem). In LPT of dispersed two-phase flow, the droplets are assumed to be points which move in the continuous gas phase. If the grid is refined in this case, the point approximation weakens as the grid spacing approaches the droplet size. No continuous phase is left in the cell, and the computation of local gas properties at that point cannot be justified. It can therefore not be proven that the differential equations are recovered in the limit of zero cell size.

A region which clearly violates the model assumptions is the near-field of the liquid jet. The atomization of a liquid jet to fine droplets is a research objective as it is still debated if an intact liquid core exists. The dense spray in the jet region is difficult to penetrate with current optical diagnostics. Likewise, the dense spray region leads to modeling difficulties with current modeling techniques. Therefore understanding of the two-phase

flow phenomena in the jet region is limited. The modeling difficulties of LPT in the jet region are one of the topics of this work. If there was a clearly defined interface between liquid- and gas phase, one could track it using the volume of fluid (VOF) method as it is attempted in Arienti et al. (2005). However, the existence of such an interface is unclear and the computational cost of the VOF method is large. Therefore the jet is commonly modeled by so-called blob-injection (Reitz and Diwakar, 1987), i.e. as a succession of discrete droplets or cylindrical slices with a size on the order of the nozzle diameter, e.g. in Rachner et al. (2002), Madabhushi (2003), Khosla and Crocker (2004), Nguyen and Karagozian (1992), or Wu et al. (1997). Breakup models are used to model stripping of small droplets off the jet and atomization. The discrete large droplets are tracked in Lagrangian coordinates assuming the droplets are isolated and spherical. These model premises, however, are violated in the jet region. Moreover, it is easy to estimate the droplet radii in the blob-injection model are at least on the order of the Kolmogorov scales of the turbulent channel flow, violating an assumption of uniform flow in the equation of motion of the droplets. Lastly, the nozzle size and therefore the size of the droplets at injection is on the order of the size of the numerical cells. This means that the blob-injection model is inherently inconsistent as described above.

## 2. Case description

The baseline case has been investigated in the literature using phase-Doppler anemometry (PDA) (Becker and Hassa, 2002). The channel is shown in Fig. 1. The case is selected as it uses kerosene spray and the pressure is elevated to $p = 6$ bar. The nozzle diameter is $D = 0.45$ mm, the channel height is $H = 40$ mm, the gas velocity is $U = 100$ m/s. The gas phase Reynolds number is $Re = 260000$, based on the gas velocity, the channel height, and the gas phase kinematic viscosity $\nu_g$ (Eq. (1)). The momentum flux ratio, defined in Eq. (2), of the baseline case is $J = 6$

$$Re = \frac{UH}{\nu_g} \tag{1}$$

$$J = \frac{(\rho U^2)_{\text{jet}}}{(\rho U^2)_{\text{crossflow}}} \tag{2}$$

The channel has dimensions of $(x, y, z) = (90, 90, 540)$ nozzle diameters. The transverse jet is injected at $(45, 0, 405)$ nozzle diameters. At the upper and lower wall no-slip boundary conditions are applied, in lateral direction periodic boundary conditions. The flow is fully turbulent at the jet injection point. This is always difficult to achieve due to the finite length of any computational domain. Therefore, two channels are simulated in the present case, each 270 nozzle diameters long. The first channel simply simulates a single-phase turbulent channel flow. It has periodic conditions also in the streamwise direction. Its sole purpose is to compute inlet boundary conditions for the second channel. This second channel contains the spray jet. The inlet boundary condition of the second channel is therefore a fully developed turbulent flow, both in profile and in spectral content. The outflow of the second channel has a flux conserving zero-gradient boundary condition. The initial parcel positions and velocities are set. The initial Sauter mean diameter (SMD) is set in each case. The droplets have a log-normal distribution in which the root mean square is 20% of the droplet size. The droplets are assumed to bounce elastically at the walls, while the lateral direction is assumed to be periodic. Droplets are destroyed at the outlet of the flow domain.

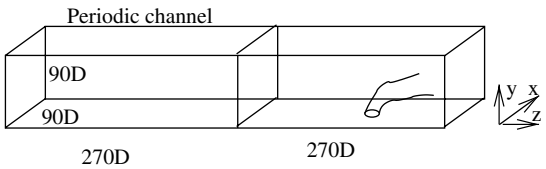


Fig. 1. Geometry of the spray jet in crossflow.

## 3. Governing equations and numerical methods

The numerical simulation is done in an Euler/Lagrange framework. Two-way coupling between the continuous and dispersed phases is applied for momentum, energy, and mixture fraction transport equations.

### 3.1. Continuous phase

The non-dimensional continuity (Eq. (3)) and momentum (Eq. (4)) equations for incompressible flow of Newtonian fluids with constant diffusivities are described in Eulerian framework. Additionally, transport equations for energy (Eq. (5)) and mixture fraction are solved (Eq. (6)) in the hot flow case with evaporation. These equations are valid for low Mach numbers (Poinsot and Veynante, 2001)

$$\frac{\partial u_j}{\partial x_j} = 0 \tag{3}$$

$$\frac{\partial u_i}{\partial t} + u_j \frac{\partial u_i}{\partial x_j} = -\frac{\partial p}{\partial x_i} + \frac{1}{Re} \frac{\partial^2 u_i}{\partial x_j^2} + \dot{F}_{s,i} \tag{4}$$

$$\frac{\partial h}{\partial t} + u_j \frac{\partial h}{\partial x_j} = \frac{1}{RePr} \frac{\partial^2 h}{\partial x_j \partial x_j} + \dot{Q}_s \tag{5}$$

$$\frac{\partial Z}{\partial t} + u_j \frac{\partial Z}{\partial x_j} = \frac{1}{ReSc} \frac{\partial^2 Z}{\partial x_j \partial x_j} + \dot{Z}_s \tag{6}$$

Repeated indices in a term imply summation over all three coordinate directions $x_j$ (Einstein summation convention). $u_j$ are the gas phase velocities, $p$ the gas phase pressure, $Re$ is the Reynolds number of the gas phase (see Eq. (1)). $Sc$ and $Pr$ numbers are the Schmidt and Prandtl numbers of the evaporated fuel, respectively. They are assumed to be unity which means that momentum, heat, and mass are supposed to diffuse equally fast, $h$ is the enthalpy of the gas and $Z$ the mixture fraction.

In the cases without evaporation, the energy and mixture fraction transport equations are not needed due to the low Mach number assumption. The variations in density $\rho_g$ scale as the square of the Mach number $Ma, \frac{\delta\rho_g}{\rho_g} \sim Ma^2$, and the density can therefore be considered constant. This assumption results in significant savings in computer time, because no acoustic waves have to be tracked. Even though the flow is dense near the nozzle, one can still assume that the volume fraction of the gas phase is unity. It can be inferred from the average droplet spacing maps in Section 4 and Eq. (14) that the gas phase volume fraction is above 98%, except very close to the nozzle where it is 94% (below 6 nozzle diameters from the nozzle for the baseline case). The modeling error due to assuming unity volume fraction for the gas phase (point particles) is smaller than the modeling error due to the low Mach number assumption, as the Mach number is ~0.25. $\dot{F}_{s,i}, \dot{Q}_s$, and $\dot{Z}_s$ are the source terms for the momentum, energy, and mixture fraction transport equations, respectively. They provide for the coupling from the liquid phase to the gas phase and are given by the rates of change of momentum, energy, and species of all droplets in the incremental volume. This ensures global conservation of momentum, energy and fuel species. The coupling terms in energy and mixture fraction transport equations only need to be computed in the hot flow case with evaporation. The mass coupling terms can be neglected since the temperature is fairly low (400 K). The mixture fraction does not exceed 1% in the entire domain and thus the associated modeling error with neglecting the source term in the continuity equation is much smaller than the modeling error due to the low Mach number assumption

$$\dot{F}_{s,i} = -\frac{L}{U^2} \int f \rho_l \left( \frac{4}{3} \pi r_p^3 \frac{\mathrm{d}v_{p,i}}{\mathrm{d}t} + 4\pi r_p^2 \frac{\mathrm{d}r_p}{\mathrm{d}t} v_{p,i} \right) \mathrm{d}\vec{v}\,\mathrm{d}r\,\mathrm{d}T\,\mathrm{d}y\,\mathrm{d}\dot{y} \tag{7}$$

$$\dot{Q}_s = -\frac{L}{Uh_\infty} \int f \rho_l \left( 4\pi r_p^2 \frac{\mathrm{d}r_p}{\mathrm{d}t} h_{\mathrm{latent}} + \frac{4}{3} \pi r_p^3 c_p \frac{T}{\mathrm{d}t} \right) \mathrm{d}\vec{v}\,\mathrm{d}r\,\mathrm{d}T\,\mathrm{d}y\,\mathrm{d}\dot{y} \tag{8}$$

$$\dot{Z}_s = -\frac{L}{U} \int f \rho_l 4\pi_p^2 \frac{\mathrm{d}r}{\mathrm{d}t} \mathrm{d}\vec{v}\,\mathrm{d}r\,\mathrm{d}T\,\mathrm{d}y\,\mathrm{d}\dot{y} \tag{9}$$

$L$ and $U$ are the length and velocity scales of the gas phase, respectively, $\rho_l$ is the liquid density, $h_\infty$, is the reference enthalpy, $h_{latent}$ is the latent heat of vaporization, and $c_p$ the heat capacity of the liquid. The droplet distribution function f describes the number of droplets per unit volume at a position between $\vec{x}$ and $\vec{x}+\mathrm{d}\vec{x}$ which have a velocity between $\vec{v}_p$ and $\vec{v}_p+\mathrm{d}\vec{v}_p$, a temperature between $T$ and $T+\mathrm{d}T$, and a radius between $r_p$ and $r_p+\mathrm{d}r_p$ with distortion parameters between $y$ and $y+\mathrm{d}y$ and $\dot{y}$ and $y+\mathrm{d}\dot{y}$, e.g. Kuo (1986). Integration over all droplets then gives the source terms for the continuous phase equations. The distortion parameters are relevant for the TAB breakup model (O'Rourke and Amsden, 1987).

A finite difference formulation is applied on a staggered grid. The grid is stretched to improve the resolution near the walls. The spatial discretization is done with a fifth-order weighted essentially non-oscillatory (WENO) scheme (Jiang and Shu, 1996) for the convective terms to handle the strong flow field curvature near the jet injection. The diffusive terms are discretized with a fourth-order central difference scheme. The flow solver uses a third-order Runge–Kutta scheme. In LES the large scales are resolved while the small, universal scales are modeled. In this work the implicit subgrid scale (SGS) models, i.e. no explicit SGS models, for SGS turbulence and SGS mixing are applied. In the turbulence energy cascade energy is transferred from the large scales to the small scales, though there can be backscatter. SGS models describe these physical processes on the border between resolved and unresolved scales. The most important is to drain kinetic energy from the large scales which is dissipated at the smallest scales of turbulence (in the real, physical world). Any stable numerical scheme can be used for this draining of the kinetic energy from the large scales, e.g. Fureby and Grinstein (2002). The implicit model can be justified if large parts of the turbulent kinetic energy spectrum are resolved. Then the unresolved scales contain little energy which can therefore be neglected. The implicit model has been used in many LES applications and has, as the resolution improves, an increasing level of acceptance. The form of the dissipation depends on the numerical scheme. The success of the implicit model can be attributed to the fact that the discretization error is often of the same order as the subgrid scale stress terms (Gullbrand and Chow, 2003). Further discussion can be found in Sagaut (1998) or Pope (2000).

### 3.2. Dispersed phase

The dispersion of polydisperse spray droplets is computed using LPT with the stochastic parcel method (Dukowicz, 1980). Droplets are represented by computational parcels which consist of a number of droplets with identical properties.

The droplet trajectories are calculated in Lagrangian framework. The instantaneous parcel accelerations are computed from Newton's law for constant mass assuming the momentum flux due to evaporation is uniformly distributed over the droplet surface. The force due to gas phase pressure gradient, added mass, the Basset history integral, Magnus-, Saffman-, and Faxn forces are neglected. Gravitation is also neglected. There are no Mach number effects due to the treatment of the continuous phase as incompressible. Aerodynamic drag is considered to be the only non-negligible force. The droplets are assumed to be spherical, isolated, and much smaller than the Kolmogorov scales. Under these assumptions Eq. (10) describes the motion of the droplets

$$\frac{\mathrm{d}\vec{v}_p}{\mathrm{d}t} = -\frac{3}{8}\frac{\rho_g}{\rho_l}\frac{1}{r_p}C_d|\vec{v}_p-\vec{u}_g|(\vec{v}_p-\vec{u}_g) \tag{10}$$

$C_d$ is the drag coefficient, $\vec{v}_p$ and $\vec{u}_g$ are velocities of the parcels and the gas, $r_p$ is the parcel radius, and $\rho_l$ and $\rho_g$ are the densities of liquid and gas, respectively. LES offers the advantage that the large scale velocity fluctuations are resolved. The gas velocity $\vec{u}_g$ is the filtered instantaneous velocity at the droplet location. This is consistent with the LES methodology. Wang and Squires (1996) and Yeh and Lei (1981) show that the dispersion of droplets depends mainly on the large scale motion. The effect of the unresolved scales on the dispersion of the droplets is therefore neglected. $C_d$ is correlated to the parcel Reynolds number by Eq. (11) which is valid for rigid spheres. Droplets, on the other hand, can deform and there may be internal circulation of the droplet fluid (Helenbrook and Edwards, 2002; Prahl et al., 2006). Furthermore, aerodynamic four-way interaction may be important in dense sprays (Prahl et al., 2006; Holländer and Zaripov, 2005). These effects compromise the model accuracy for the estimation of the drag coefficient $C_d$

$$C_d = \begin{cases} \frac{24}{Re_p}\left(1 + \frac{1}{6}Re_p^{2/3}\right) & \text{for } Re_p \leqslant 1000 \\ 0.424 & \text{for } Re_p \geqslant 1000 \end{cases} \tag{11}$$

The parcel Reynolds number $Re_p$ is defined by Eq. (12), in which $\nu_g$ is the gas phase kinematic viscosity

$$Re_p = \frac{|\vec{v}_p - \vec{u}_g| 2 r_p}{\nu_g} \tag{12}$$

Two alternative breakup models are studied: The wave breakup model (Reitz and Diwakar, 1987) and the Taylor analogy breakup (TAB) model (O'Rourke and Amsden, 1987). The Weber number We is the ratio of the aerodynamic forces and the surface tension $\sigma$ (Eq. (13)) and is therefore a characteristic parameter for droplet breakup

$$We = \frac{\rho_g |\vec{v}_p - \vec{u}_g|^2 r_p}{\sigma} \tag{13}$$

In the wave breakup model both bag breakup and stripping breakup are taken into account. A droplet breaks up in the bag breakup mode if its Weber number $We \geqslant 6$ for longer than the life time of an unstable droplet. A droplet breaks up in the stripping mode if $We/\sqrt{Re_p} \geqslant 0.5$. In the TAB model a distortion equation is solved for each droplet. In the wave model as well as in the TAB model large Weber numbers promote droplet breakup.

The evaporation is calculated considering isolated, spherical, mono-component droplets with homogeneous temperature and constant density. No gas can be solved in the droplets or condense (Amsden et al., 1989).

Droplet collisions control the spray propagation in dense spray regions where the collision time scales are smaller than the momentum relaxation times. Depending on the ratio of surface tension and excess inertia, the droplets are thought to coalesce or bounce (Amsden et al., 1989). Droplets are assumed to be spherical.

## 4. Results

The given baseline case is investigated in several publications in which gas velocities and droplet volume fluxes are presented (Rachner et al., 2002; Becker and Hassa, 2002; Khosla and Crocker, 2004). The present simulation is compared to the experimental data of this baseline case in Salewski and Fuchs (2006), along with an estimate for the numerical accuracy. The simulation matches the experimental data within the experimental accuracy of the PDA measurements. In this section the average droplet spacing, Weber number, and Stokes number iso-contours in the center-plane are presented. As Weber and Stokes numbers and the droplet spacing are potentially sensitive to velocities and droplet diameters (see Eqs. (13) and (15)), the sensitivity to these parameters is evaluated. Moreover, the sensitivity to the breakup model, collision model, and evaporation is addressed. Mostly, one is interested in the order of magnitude of the average Weber- and Stokes numbers and the average droplet spacing, as one can estimate the deformation, momentum coupling, and droplet-interaction regime from them.

### 4.1. Droplet spacing

The average droplet spacing is defined as the mean distance $L$ between two droplets divided by the diameter $D_p$. The distribution of the average droplet spacing $L/D_p$ is shown in Figs. 2–4. For the purpose of better readability of the following figures, the jet injection point is now defined as $z/D = 0$, a simple shift in coordinates by $z/D = 405$. In Fig. 2 the injection Sauter mean diameter is SMD = 160 μm and the momentum flux ratio is varied from $J = 6$–113. In Fig. 3 the momentum flux ratio is fixed at $J = 41$ while the Sauter mean diameter is varied from SMD = 10–450 μm. Both parameter sensitivity studies are performed using the wave breakup model (Reitz and Diwakar, 1987) and a collision model (Amsden et al., 1989). Evaporation is not included. In Fig. 4 the sensitivity of the results to the breakup model, the collision model, and an evaporation model

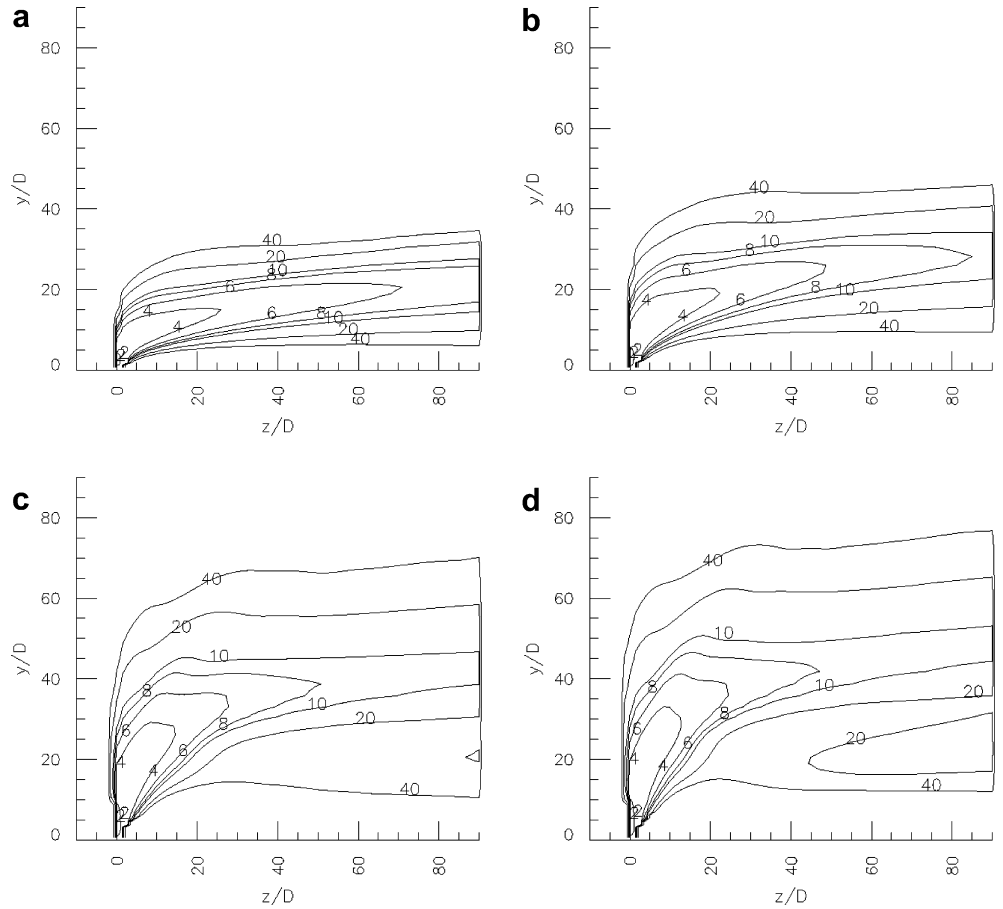


Fig. 2. Average droplet spacing for SMD = 160 μm and various momentum flux ratios, $J$. (a) $J = 6$, (b) $J = 18$, (c) $J = 73$, (d) $J = 113$.

is established for $J = 41$ and SMD = 160 μm, complementing the results in Figs. 2 and 3. The average droplet spacing $L/D_p$ is related to the liquid volume fraction $\alpha$ by Eq. (14) (Crowe et al., 1998)

$$\alpha = \frac{\pi D_p^3}{6L^3} \tag{14}$$

The assumption that the droplets can be treated as point particles that do not interact with each other (i.e. only two-way interaction is allowed) relies on large inter-droplet spacing. In the framework of two-way coupling, the drag coefficient (Eq. (11)) is independent of passers-by droplets and only depends on the droplet Reynolds number. Figs. 2–4 reveal that the average droplet spacing is as low as $L/D_p \sim 6$ in large parts of the flow field. In the baseline case Fig. 2(a) the droplet spacing is $L/D_p \sim 6$ up to 70 nozzle diameters downstream of the nozzle. It is likely that the droplets cross each other's wakes and displace fluid so that the lift- and drag coefficients are altered significantly. The aerodynamic interaction effects on the drag coefficient can be as much as 30% up to a droplet spacing $L/D_p \sim 6$ in the wake of a preceding droplet (Prahl et al., 2006). This droplet spacing corresponds to a volume fraction of about 0.002 (see Eq. (14)). This order of magnitude is supported by Elghobashi (1994) who delineates four-way from two-way coupling at volume fractions on the order of 0.001. This aerodynamic particle-particle interaction is, however, neglected in simulations in Euler/Lagrange framework, even though the low droplet spacing suggests that aerodynamic four-way interaction may be important (Rachner et al., 2002; Madabhushi, 2003; Khosla and Crocker, 2004; Nguyen and Karagozian, 1992; Wu et al., 1997). Also in other flow fields the droplet spacing may be as low as $L/D_p \sim 3$, but aerodynamic particle-particle interaction is neglected (Sankaran and Menon, 2002 or Vermodel et al., 2003). The

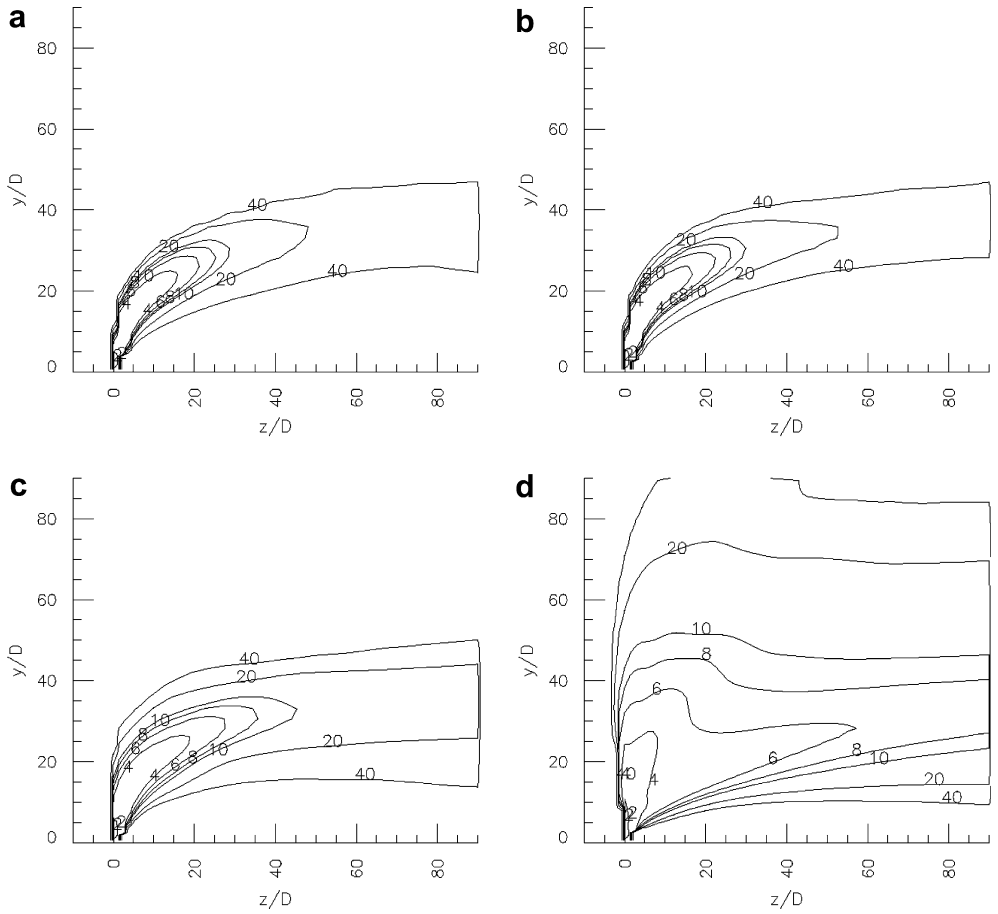


Fig. 3. Average droplet spacing for $J = 41$ and various injection Sauter mean diameters SMD. (a) SMD = 10 μm, (b) SMD = 20 μm, (c) SMD = 80 μm, (d) SMD = 450 μm.

droplet spacing especially in the jet region is so low that neglecting collision and aerodynamic inter-droplet interaction is doubtful. Fig. 2 shows that the droplet spacing in the center-plane in the far-field becomes larger for increased momentum flux ratio. The increased momentum flux ratio results in a stronger counter-rotating vortex pair (CVP) which in turn increases the lateral dispersion of the droplets, leaving fewer droplets in the center-plane. Off the center-plane the increased lateral dispersion leads to smaller droplet spacing for high momentum flux ratio (Salewski and Fuchs, 2006). Even for the highest investigated momentum flux ratio $J = 113$ the region of small droplet spacing ($L/D_p \sim 6$, say) extends to 40 nozzle diameters upwards. Fig. 3 deals with the parameter sensitivity to the injection SMD. In the blob-injection model (Reitz and Diwakar, 1987) droplets are on the order of the nozzle size (SMD = 450 μm, Fig. 3(d)), but in principle one could also assume smaller droplets. The droplet spacing is strongly dependent on the injection droplet size. The reason is similar to the reason for varying momentum flux ratio: Droplets with small injection SMD have a large ratio of aerodynamic forces to inertial forces since aerodynamic forces scale with $SMD^2$ whereas inertial forces scale with $SMD^3$. Therefore droplets with small radii have small Stokes numbers (see Fig. 9). They induce a strong CVP which disperses the droplets outwards fast, again owing to their small Stokes numbers. As in the case of varying momentum flux ratio, fewer droplets in the center-plane mean, of course, more droplets off the center-plane. Fig. 4 investigates the impact of submodels which are used. Comparing Fig. 4(a) and (b), which show the droplet spacing for the wave breakup model with and without a collision model, one notes that peak droplet densities are reduced in the computation with the collision model. This is due to enhanced lateral dispersion from the center-plane. Moreover, the droplet trajectory based on the average droplet spacing is higher if a

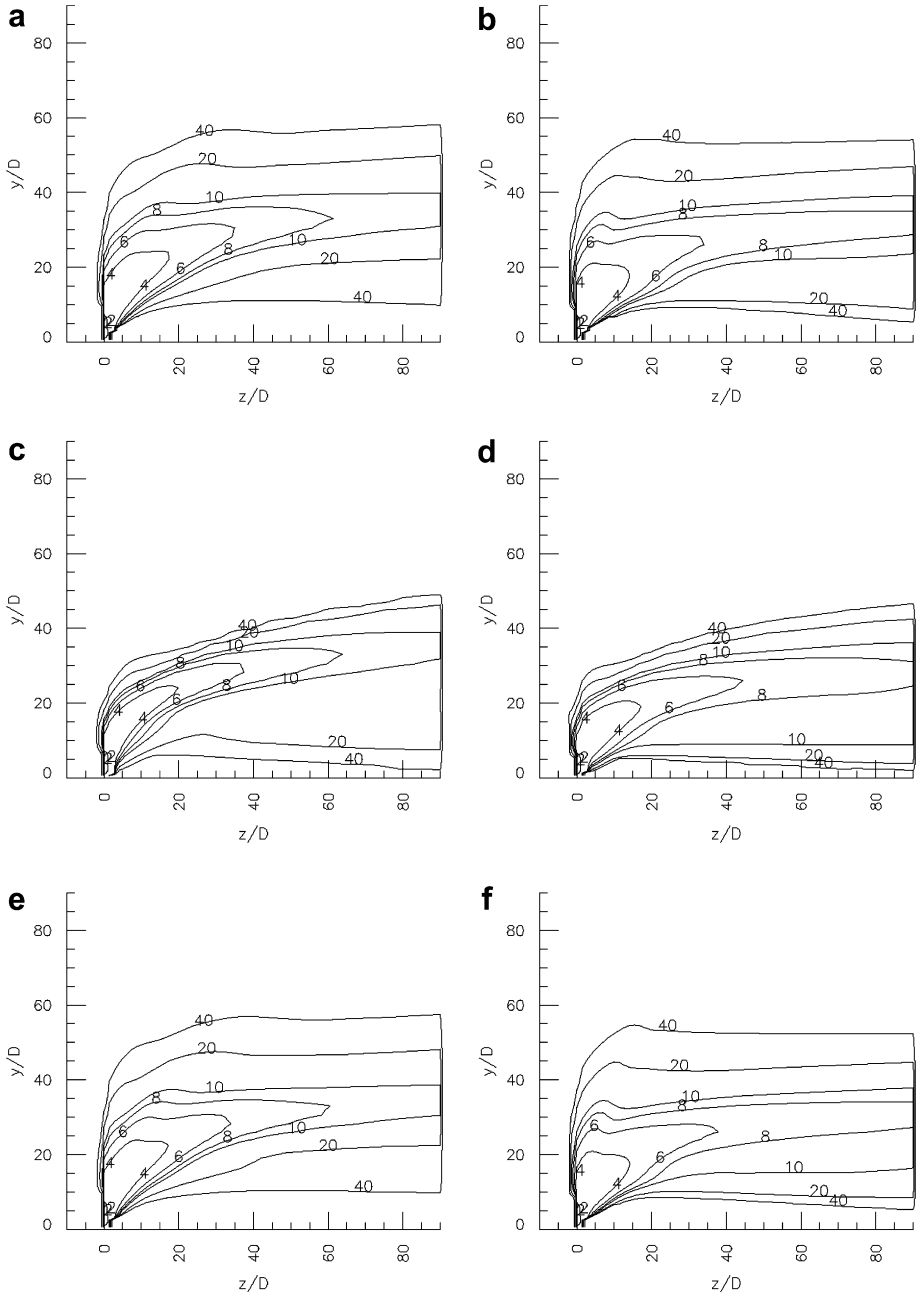


Fig. 4. Average droplet spacing for wave breakup and TAB model, with and without collision and evaporation, $J = 41$ and SMD = 160 μm. (a) Wave breakup, with collision, (b) wave breakup, no collision, (c) TAB, with collision, (d) TAB, no collision, (e) wave breakup, with collision and evaporation, (f) wave breakup, no collision, but evaporation.

collision model is used. If no collision model is used, small droplets can leave the spray jet and are blown in the wake of the jet. In this case the droplet spacing in the wake of the jet close to the wall is lower. The collision model tends to prevent small droplets to leave the spray as momentum is exchanged with the large droplets and the droplet diameter increases due to coalescence. The same is true for the TAB model (Fig. 4(c) and (d)), but the faster breakup of the large droplets leads to smaller spray penetration. In Fig. 4(e) and (f) evaporation is computed for a temperature of 400 K. At this temperature small droplets fully vaporize, increasing the average droplet spacing. Up to this temperature, however, the droplet spacing is not affected significantly.

To summarize, in a wide range of conditions and with a wide range of models four-way coupling of the droplets may be important as the droplet cannot be regarded as isolated.

### 4.2. Droplet sphericity

Figs. 5–7 are iso-curves of the aerodynamic Weber number (Eq. (13)). Analog to Figs. 2–4, in Fig. 5 the momentum flux is varied at SMD = 160 μm, in Fig. 6 the injection SMD is varied at $J = 41$, and Fig. 7 studies the impact of the submodels at $J = 41$ and SMD = 160 μm. The Weber number iso-curves in the baseline case in Fig. 5(a) show that the Weber numbers not only in the jet region but also up to 40 nozzle diameters downstream are on the order of one. Weber numbers on this order imply that the aerodynamic forces on the droplets are of the same magnitude as the surface tension forces. Under this aerodynamic strain the droplets are severely distorted (Prahl et al., 2006; Helenbrook and Edwards, 2002). The model assumption that the droplets are spherical in Eqs. (10) and (11) is inconsistent with the results. An attempt to take non-sphericity into account is to work with equivalent spheres and model the drag coefficient accordingly, such that non-spherical droplets have an altered drag coefficient. A relation which correlates the drag coefficient to the Reynolds and Weber numbers is suggested in Helenbrook and Edwards (2002). Since the Weber number is proportional to the droplet diameter and the square of the relative velocity (Eq. (13)), sensitivity studies of the results are performed with respect to the injection velocity and the injection SMD at conditions relevant to gas turbines. In Fig. 5 it is shown that the average aerodynamic Weber numbers in the jet region are on the order of $We \sim 10$

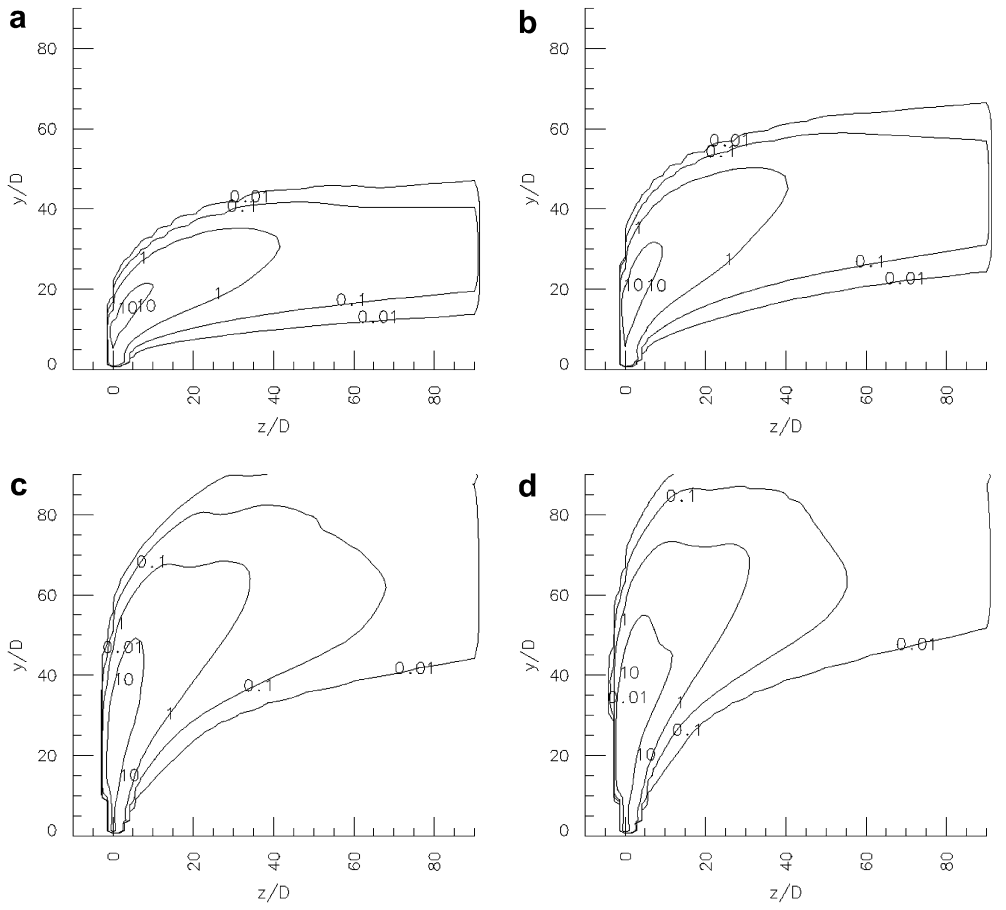


Fig. 5. Average Weber numbers for SMD = 160 μm and various momentum flux ratios $J$. (a) $J = 6$, (b) $J = 18$, (c) $J = 73$, (d) $J = 113$.

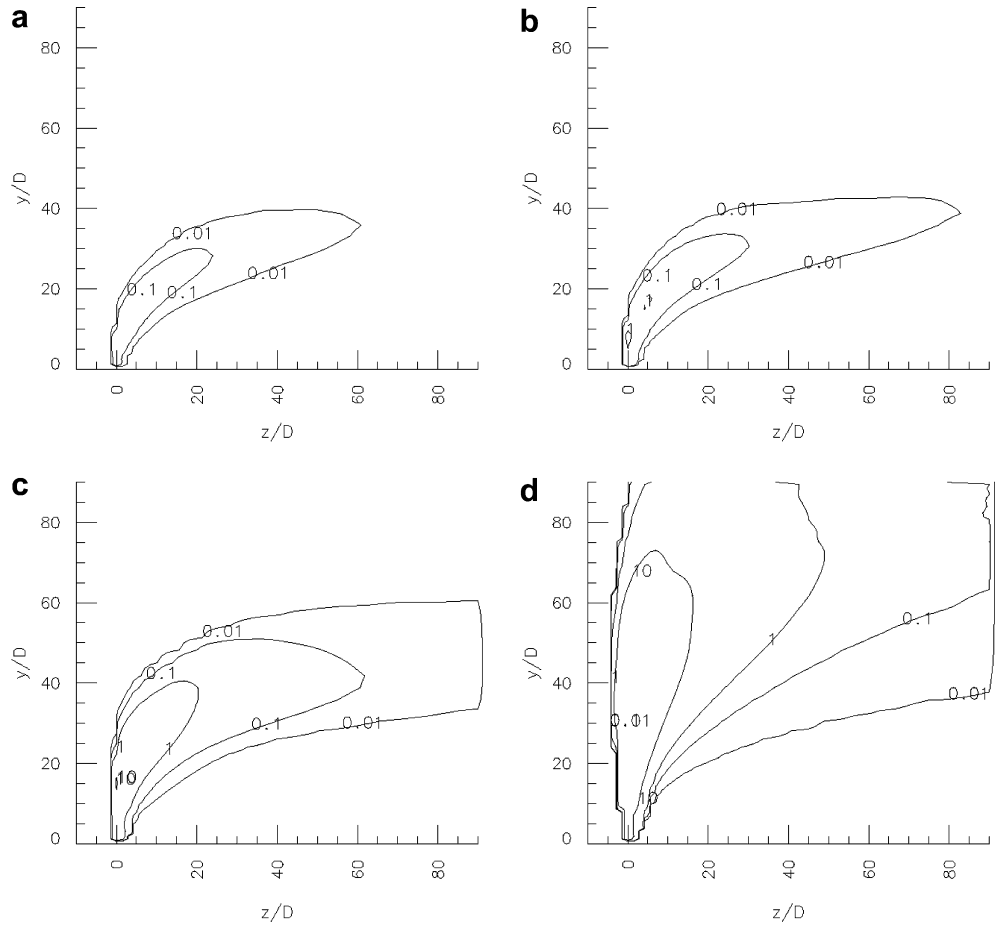


Fig. 6. Average Weber numbers for $J = 41$ and various injection Sauter mean diameters SMD. (a) SMD = 10 μm, (b) SMD = 20 μm, (c) SMD = 80 μm, (d) SMD = 450 μm.

for momentum flux ratios from $J = 6$–113. This is due to the fact that the channel flow velocity is larger than the liquid jet velocity. The region of severe droplet distortion lies inside the iso-curve $We = 1$. For all investigated momentum flux ratios $J = 6$–113 this region extends to at least 40 nozzle diameters away from the nozzle. The impact of the injection droplet size is more significant (Fig. 6): If the injection Sauter mean diameter is SMD = 10 μm the Weber numbers are on the order of $We \sim 0.1$ up to about 20 nozzle diameters whereas for SMD = 450 μm (the nozzle size) the Weber numbers are on the order of $We \sim 10$ more than 70 nozzle diameters away from the nozzle. Fig. 7 shows the impact of submodels used in the calculation. In the case of the wave breakup model (Fig. 7(a), (b), (e), and (f)) the Weber numbers are larger than for the TAB model (Fig. 7(c) and (d)). In the calculation using the wave breakup model large droplets penetrate far into the cross-flow, giving a large region of large average Weber numbers. With a TAB model these break up fast and do not penetrate as far. For the TAB model the Weber numbers are similar with or without collision model. For the wave breakup model, however, the cases without collision model show small droplets leaving the spray as explained above. If the temperature is set to 400 K, the average Weber numbers become slightly smaller due to the smaller droplet radii (Fig. 7(e) and (f)). At this temperature the effect is still small. In all cases it is important to note that there are large regions in the flow field, where the assumption of spherical droplets cannot be justified, and no consistent solution is obtained due to these regions. Figs. 5–7 also give an estimate on where PDA can be applied. As PDA relies on the assumption that droplets are spherical, one can estimate that for accurate PDA measurements one should be well in the far-field of the JICF. Another important

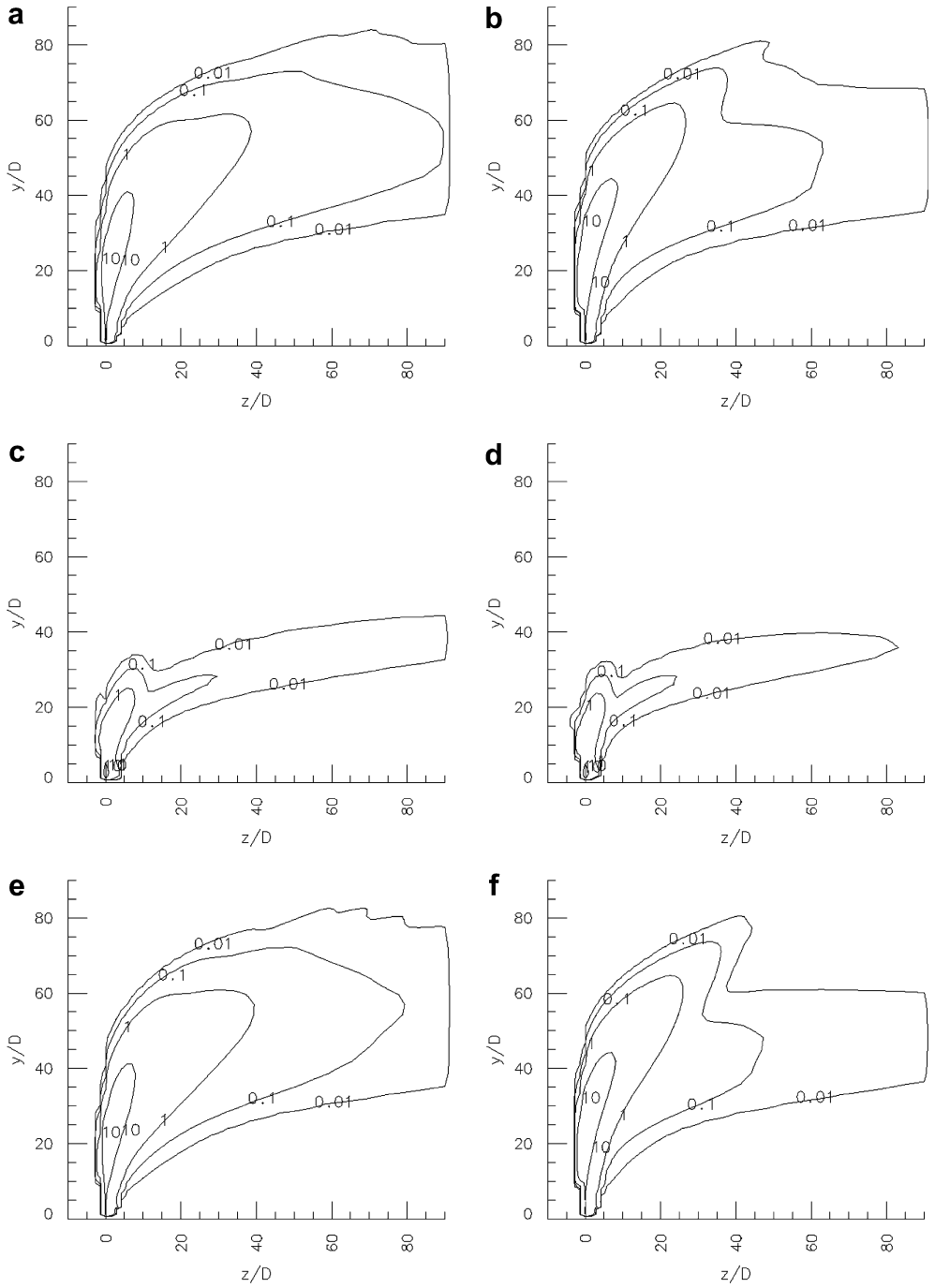


Fig. 7. Average Weber numbers for wave breakup and TAB model, with and without collision and evaporation, $J = 41$ and SMD = 160 μm. (a) Wave breakup, with collision, (b) wave breakup, no collision, (c) TAB, with collision, (d) TAB, no collision, (e) wave breakup, with collision and evaporation, (f) wave breakup, no collision, but evaporation.

implication regards the commonly used atomization model to model liquid jets as a succession of discrete droplets or cylindrical slices with a size on the order of the nozzle diameter, e.g. Rachner et al. (2002), Madabhushi (2003), Khosla and Crocker (2004), Nguyen and Karagozian (1992) and Wu et al. (1997). From Figs. 5–7 it is clear that the premise that droplets are spherical is violated, and the model premise for blob-injection is violated in any case.

### 4.3. Inter-phase momentum coupling

Elghobashi (1994) summarizes the regimes in which one-way, two-way, and four-way coupling are important. Two-way coupling describes the mutual influence of the continuous and dispersed phases. A non-dimensional number which characterizes this interaction is the Stokes number St (Eq. (15)). It is the ratio of the momentum response time $\tau_v$, which is a time scale inherent to Eq. (10), and a flow time scale $\tau_f$

$$St = \frac{\tau_v}{\tau_f} \tag{15}$$

For a spherical droplet the momentum response time can be estimated by Eq. (16) from the liquid and gas densities $\rho_l$ and $\rho_g$, the parcel diameter $D_p$, and the kinematic viscosity of the gas phase $v_g$

$$\tau_v = \frac{\rho_l}{\rho_g} \frac{D_p^2}{18 v_g} \tag{16}$$

The relevant flow time for large scale dispersion of the droplets is the integral time scale which is estimated from the integral length and velocity scales $l_0$ and $u_0$, respectively

$$\tau_f = \frac{l_0}{u_0} = \frac{0.04\ \mathrm{m}}{100\ \mathrm{m/s}} = 0.0004\ \mathrm{s} \tag{17}$$

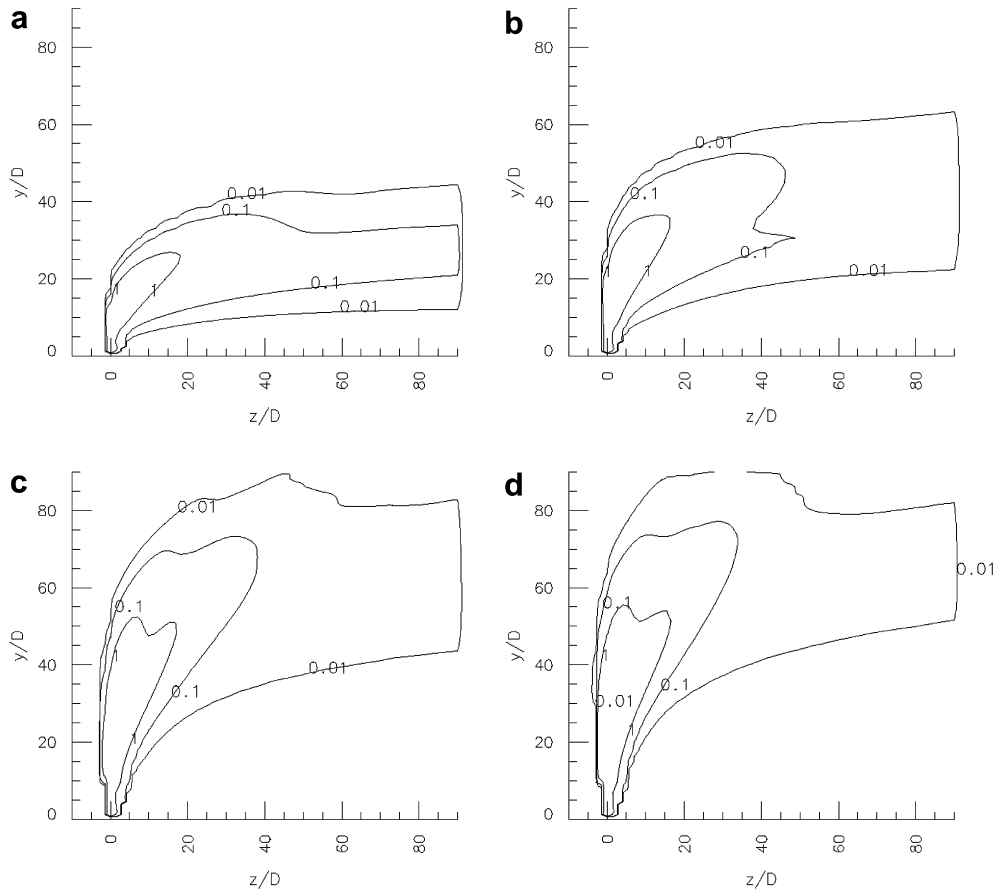


Fig. 8. Average Stokes numbers for SMD = 160 μm and various momentum flux ratios $J$. (a) $J = 6$, (b) $J = 18$, (c) $J = 73$, (d) $J = 113$.

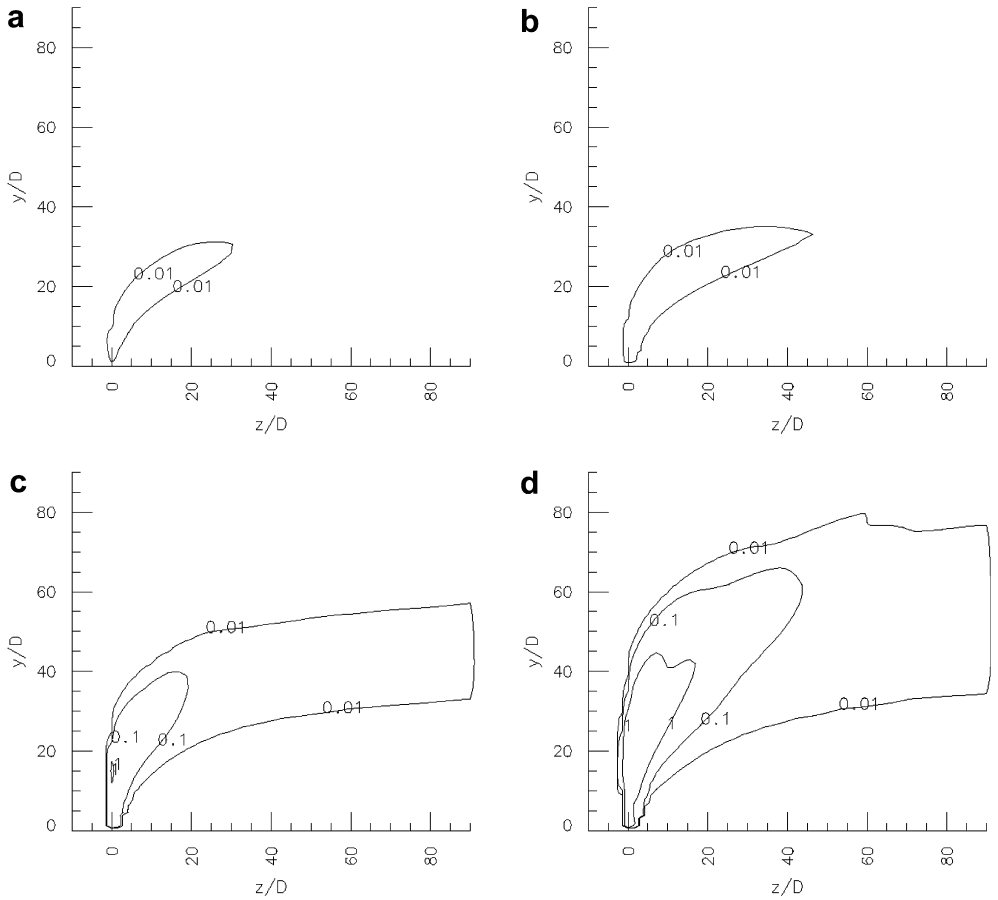


Fig. 9. Average Stokes numbers for $J = 41$ and various injection Sauter mean diameters SMD. (a) SMD = 10 μm, (b) SMD = 20 μm, (c) SMD = 80 μm, (d) SMD = 450 μm.

If $St \gg 1$, the momentum response time $\tau_v$ is large as compared to the flow time scale $\tau_f$ and the droplet trajectory is marginally affected by the flow. Contrarily, if $St \ll 1$, the droplet reacts quickly and the droplet follows the local fluid flow. The Stokes number iso-curves (Figs. 8–10) provide information about the momentum transfer and the dispersion. The momentum transfer between the dispersed phase and the continuous phase is delayed for large Stokes numbers. The slip velocities for large Stokes numbers are large. The region with large Stokes number extends further for larger momentum flux ratio (Fig. 8). In the jet region, the Stokes number is highly dependent on the injection SMD as Fig. 9 reveals. Eq. (16) shows that the Stokes number is sensitive to the droplet diameter, $St \sim D_p^2$. In Fig. 9(a) and (b) the Stokes number is smaller than $St \sim 1$, suggesting large momentum transfer rates between the droplets and the continuous phase. In Fig. 9(c) and (d), on the other hand, the Stokes number in the jet region is on the order of $St \sim 1$ or more. This means that the momentum coupling between the two phases is weak, even though the large liquid volume fraction suggests that two-way coupling or even four-way coupling is important Elghobashi (1994). However, droplets change slowly their velocity. Therefore, the source terms in the momentum equations are small in this region and the induced velocities in the continuous phase are small, resulting in a weak CVP. The large Stokes number in the jet region is the also reason that no recirculation bubble forms in the wake of the liquid jet. This is another weakness of the modeling of atomization by injecting large droplets. The region of large Stokes numbers extends further for computations using the wave breakup model (Fig. 10(a) and (b)) than with the TAB model (Fig. 10(c) and (d)). With the TAB model all large droplets break up which rapidly decreases the Stokes number. The momentum coupling is therefore stronger using a TAB model. As before, evaporation has not a strong effect for temperatures up to 400 K (Fig. 10(e) and (f)) and decreases the Stokes numbers slightly.

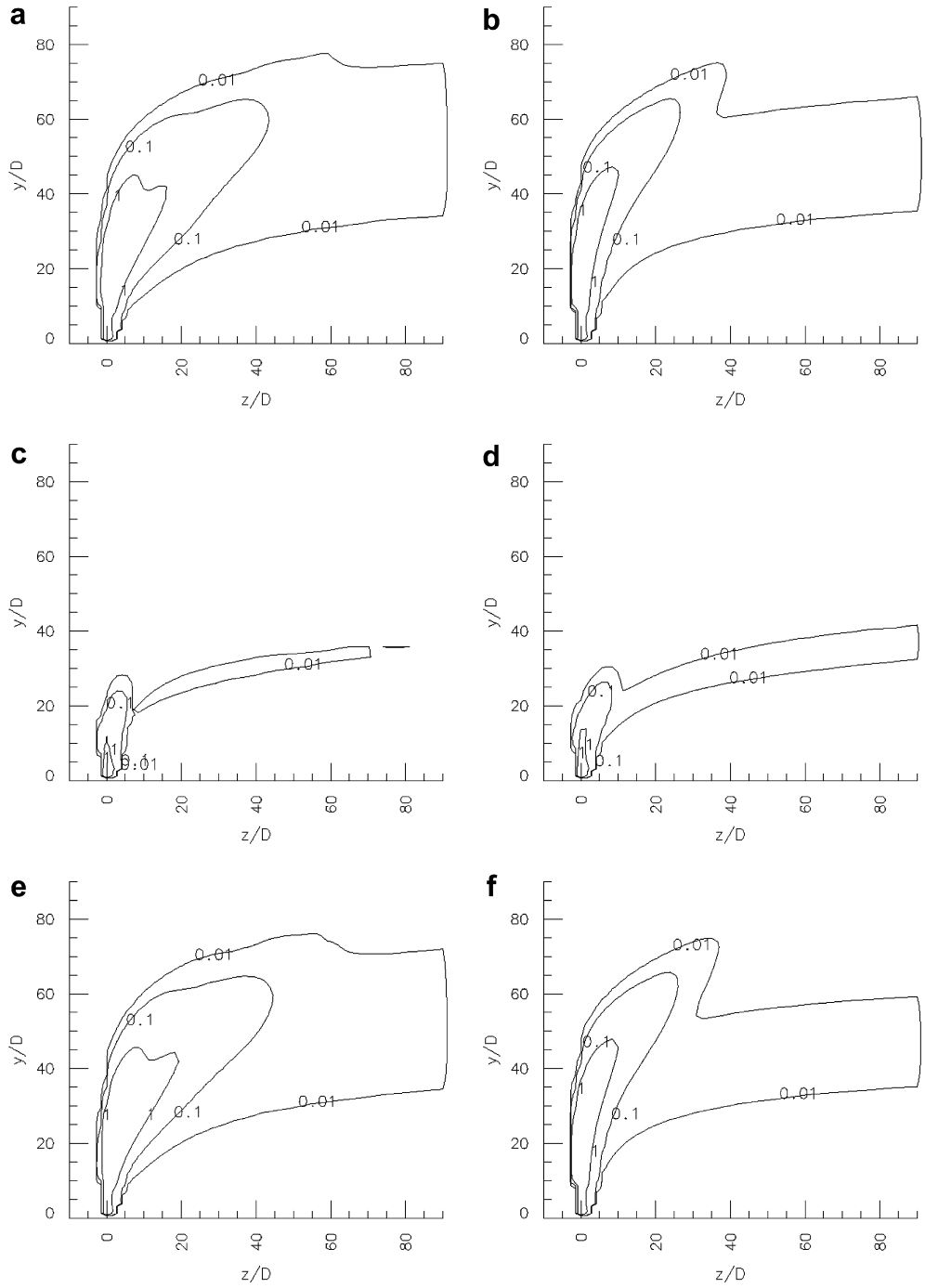


Fig. 10. Average Stokes numbers for wave breakup and TAB model, with and without collision and evaporation, $J = 41$ and SMD = 160 μm. (a) Wave breakup, with collision, (b) wave breakup, no collision, (c) TAB, with collision, (d) TAB, no collision, (e) wave breakup, with collision and evaporation, (f) wave breakup, no collision, but evaporation.

## 5. Conclusions

Regions with apparent inconsistencies of some of the underlying assumptions used with LPT are clearly detected. Such inconsistencies are observed by analysis of average Weber- and Stokes numbers, and the

average droplet spacing. The extent of regions of inconsistency are larger when turbulence related fluctuations are added. The inconsistencies are most significant in the near-field of the jet in crossflow. However, it is shown that not only in the vicinity of the jet but also further downstream in the far-field common model assumptions are not valid. The low droplet spacing not only in the jet region but also far away from the nozzle suggests that four-way coupling is probably needed if accuracy is to be maintained. To regard the particles as isolated mathematical point-objects is therefore questionable in large regions of the flow field. Secondly, the Weber numbers not only in the jet region but also far away from the jet are of order one and imply droplet deformation and varying drag coefficients. Thirdly, the Stokes numbers in the jet region are large, if large droplets are injected. Therefore, the two-way coupling does not account correctly for the momentum exchange between the continuous and the dispersed phases. These inconsistencies remain for a wide range of momentum flux ratios and injection droplet diameters. As indicated in the paper, one could improve the accuracy of LPT by modifying the assumed relations for drag and lift and account for neighboring droplets.

## Acknowledgements

The project work was supported by the Swedish Energy Agency (STEM) within the TPE program. Computational recourses were provided by LU-NARC computing center at Lund University and HPC2N facilities within the SNAC/SNIC allocation program.

## References

Amsden, A.A., O'Rourke, P.J., Butler, T.D., 1989. KIVA-II: a computer program for chemically reactive flows with sprays. Technical Report LA-11560-MS, Los Alamos National Laboratory.

Arienti, M., Madabhushi, R.K., Van Slooten, P.R., Soteriou, M.C., 2005. Numerical simulation of liquid jet characteristics in a gaseous crossflow. In: ILASS Americas, 18th Annual Conference on Liquid Atomization and Spray Systems, pp. 1–6.

Becker, J., Hassa, C., 2002. Breakup and atomization of a kerosene jet in cross-flow at elevated pressure. Atomization Sprays 11, 49–67.

Caraeni, D., Bergström, C., Fuchs, L., 2000. Modeling of liquid fuel injection, evaporation and mixing in a gas turbine burner using large eddy simulation. Flow Turbul. Combust. 65, 223–244.

Crowe, C., Sommerfeld, M., Tsuji, Y., 1998. Multiphase Flows with Droplets and Particles. CRC Press.

Dukowicz, J.K., 1980. A particle-fluid numerical model for liquid sprays. J. Comput. Phys. 35, 229–253.

Elghobashi, S., 1994. On predicting particle-laden turbulent flows. Appl. Sci. Res. 52, 309–329.

Fureby, C., Grinstein, F.F., 2002. Large eddy simulation of high-Reynolds free and wall-bounded flows. J. Comput. Phys. 181, 68–97.

Ghosh, S., Hunt, J.C.R., 1998. Spray jets in a cross-flow. J. Fluid Mech. 365, 109–136.

Gullbrand, J., Chow, F.K., 2003. The effect of numerical errors and turbulence models in large-eddy simulations of a channel flow, with and without explicit filtering. J. Fluid Mech. 495, 323–341.

Helenbrook, B.T., Edwards, C.F., 2002. Quasi-steady deformation and drag of uncontaminated liquid drops. Int. J. Multiphase Flow 28, 1631–1657.

Holländer, W., Zaripov, S.K., 2005. Hydrodynamically interacting droplets at small Reynolds numbers. Int. J. Multiphase Flow 31, 53–68.

Jiang, G.-S., Shu, C.-W., 1996. Efficient implementation of weighted ENO schemes. J. Comput. Phys. 126, 202–228.

Khosla, S., Crocker, D.S., 2004. CFD modeling of the atomization of plain liquid jets in crossflow for gas turbine applications, GT2004-54269. In: ASME Turbo Expo 2004 Proceedings.

Kuo, K.K.-Y., 1986. Principles of Combustion. John Wiley & Sons.

Madabhushi, R.K., 2003. A model for numerical simulation of breakup of a liquid jet in crossflow. Atomization Sprays 13, 413–424.

Nguyen, T.T., Karagozian, A.R., 1992. Liquid fuel jet in subsonic crossflow. J. Propul. Power 8, 21–29.

O'Rourke, P.J., Amsden, A.A., 1987. The TAB method for numerical calculation of spray breakup. SAE Technical Paper 872089.

Poinsot, T., Veynante, D., 2001. Theoretical and Numerical Combustion. R.T. Edwards,Inc., ISBN 1-930217-05-6.

Pope, S.B., 2000. Turbulent Flows. Cambridge University Press.

Prahl, L., Revstedt, J., Fuchs, L., 2006. Interaction among droplets in a uniform flow at intermediate Reynolds numbers, AIAA-2006-0295. In: 44th AIAA Aerospace Science Meeting Proceedings. ISBN 1-56347-807-2.

Rachner, M., Becker, J., Hassa, C., Doerr, T., 2002. Modelling of the atomization of a plain liquid fuel jet in crossflow at gas turbine conditions. Aerospace Sci. Technol. 6, 495–506.

Reitz, R.D., Diwakar, R., 1987. Structure of high-pressure fuel sprays. SAE Technical Paper 870598.

Sagaut, P., 1998. Large Eddy Simulation for Incompressible Flows. Springer-Verlag, ISBN 3-540-67890-5.

Salewski, M., Fuchs, L., 2006. Dispersion of circular, non-circular, and swirling spray jets in crossflow. In: Lamballais, E., Friedrich, R., Geurts, B.J., Metais, O. (Eds.), Direct and Large-Eddy Simulation VI (ERCOF-TAC Series). Springer, ISBN 1-4020-4909-9.

Sankaran, V., Menon, S., 2002. LES of spray combustion in swirling flows. J. Turbulence 3, 1–23.

Schmidt, D.P., Rutland, C.J., 2000. A new droplet collision algorithm. J. Comput. Phys. 164, 62–80.

Torres, D.J., O'Rourke, P.J., Amsden, A.A., 2003. A discrete multicomponent fuel model. Atomization Sprays 13, 131–172.
Vermodel, O., Bédat, B., Simonin, O., Poinsot, T., 2003. Numerical study and modelling of turbulence modulation in a particle laden slab flow. J. Turbulence 4, 1–39.
Wang, Q., Squires, K.D., 1996. Large eddy simulation of particle deposition in a vertical turbulent channel flow. Int. J. Multiphase Flow 22, 667–683.
Wu, P.-K., Kirkendall, K.A., Fuller, R.P., Nejad, A.S., 1997. Breakup processes of liquid jets in subsonic crossflows. J. Propul. Power 13, 64–73.
Yeh, F., Lei, U., 1981. On the motion of small particles in a homogeneous isotropic flow. Phys. Fluids 3, 2571–2586.